



Real-time multiple-particle tracking: applications to drug and gene delivery

Junghae Suh^a, Michelle Dawson^b, Justin Hanes^{a,b,*}

^aDepartment of Biomedical Engineering, The Johns Hopkins University, 3400 N. Charles St., Baltimore MD, 21218, USA

^bDepartment of Chemical and Biomolecular Engineering, The Johns Hopkins University, 3400 N. Charles St., Baltimore MD, 21218, USA

Received 12 May 2004; accepted 5 August 2004

Abstract

Complex biological environments, such as the cell cytoplasm or the mucus lining the airways of the lungs, can pose significant barriers to efficient therapeutic drug and gene delivery. Biological barriers are particularly important in controlled drug delivery applications that utilize a large carrier particle, such as a liposome or a polymer micro- or nanosphere. The dynamic transport of particulate drug and gene delivery vehicles through these barriers is poorly understood, having been primarily studied with static methods in the past. Recently, the transport of synthetic drug and gene carriers has been investigated quantitatively with real-time particle tracking technology, providing new insight into particle behavior in complex biological environments that is guiding rational improvements in particle design. This review briefly highlights basic principles of particle tracking and its application to elucidate important phenomena that limit effective particulate drug and gene delivery. © 2004 Elsevier B.V. All rights reserved.

Keywords: Drug delivery; Gene delivery; Multiple-particle tracking; Intracellular; Mucus; Diffusion; Transport; Rheology

Contents

1. Introduction	64
2. Intracellular barriers	65
2.1. Properties of cell cytoplasm.	65
2.2. Active transport of nonviral vectors.	66
2.3. Subdiffusive and immobile vectors	66
2.4. Rapid perinuclear accumulation of gene vectors	67

* Corresponding author. Department of Chemical and Biomolecular Engineering, The Johns Hopkins University, 3400 N. Charles St., Baltimore MD, 21218, USA. Tel.: +1 410 516 3484; fax: +1 410 516 5510.

E-mail address: hanes@jhu.edu (J. Hanes).

3.	Extracellular barriers	68
3.1.	Particle transport in human cystic fibrosis (CF) mucus	68
3.1.1.	Properties of CF mucus	68
3.1.2.	Heterogeneous particle transport through CF mucus	68
3.1.3.	Micro- and macrorheology of CF mucus.	68
3.1.4.	Effects of mucolytic agents.	70
3.2.	Particle transport in gastrointestinal mucus	70
4.	Other applications	71
4.1.	Viral gene delivery vectors	71
4.2.	Characterizing cell cytoplasm	71
4.3.	Motion of plasma membrane components	71
5.	Particle tracking technology: a brief tutorial	71
5.1.	Time scale	72
5.2.	Individual vs. ensemble transport properties	73
5.3.	Transport modes	73
5.3.1.	Simple diffusion	74
5.3.2.	Anomalous subdiffusive transport	74
5.3.3.	Corralled motion	74
5.3.4.	Active transport	74
5.3.5.	Immobile	74
5.4.	Diffusivities	75
5.4.1.	Microscopic diffusion	75
5.4.2.	Mesosopic diffusion.	75
5.4.3.	Macroscopic diffusion	76
5.5.	2D v. 3D tracking	76
5.6.	Tracking resolution	76
6.	Conclusions	77
	References	77

1. Introduction

Effective drug and gene delivery to target cells is often limited by inefficient particle transport through complex extra- and intracellular biological environments [1]. For example, drug/gene particulate carriers delivered to the gastrointestinal (GI) tract or to the lungs via inhalation must be capable of traversing mucus barriers designed to trap foreign particulates and prevent their transport to underlying cell surfaces [2,3]. Mucus depletion of cell monolayers typically dramatically improves gene transfection of cells with nonviral vectors [4], underscoring the importance of the mucus barrier. Once in cells, gene vectors must traverse the highly crowded cytoplasm, congested with macromolecules and organelles, to reach the nucleus [5]. The sparse quantitative investigations of these barriers have focused largely on bulk particle transport properties.

In these studies, individual particle interactions with their biological environment remain a black box. Additionally, the dynamic interaction of drug/gene delivery vectors with components in the extra- and intracellular environments have often been overlooked. Limited understanding of barriers to efficient delivery hampers the rational design of improved vectors.

To address these issues, real-time multiple-particle tracking (MPT) technology has recently been applied to the study of drug and gene carrier delivery through biological environments [2,3,5,6]. As the name implies, multiple-particle tracking involves tracking the microscopic motion of tens of individual particles simultaneously in real-time using video microscopy. Particle tracking technology is valuable in obtaining information on how, and how fast, particles move in various environments. Data obtained at the individual particle level can be

critical in revealing particle–environment interactions and cellular processes that control overall bulk transport properties. This information may then be used to deduce important properties of the environment itself, such as its viscoelasticity [7] or pore sizes [8]. Using time-resolved trajectories of particles, quantitative information (such as diffusivity and velocity) and qualitative information (such as directionality and transport mode) can be obtained. Furthermore, the data from hundreds of individual particles provides important statistical insights of the population as a whole. Thus, MPT allows the analysis of particle transport from the single-particle level, to the transport of subclasses of particles, and finally, to the ensemble-averaged transport properties of the bulk population.

By investigating the interactions and transport rates of vectors quantitatively at the microscopic scale, new insights have emerged that are guiding the development of more effective delivery systems. For example, tracking individual drug carriers in mucus revealed a large percentage of nanoparticles are immobile, thereby driving the design of new carriers that are smaller (to avoid entropic caging by mucus components) and/or less adhesive to mucus (by altering particle surface chemistry) [3].

Intracellular particle tracking studies of polyethylenimine (PEI)/DNA nanocomplexes revealed these gene vectors achieve rapid perinuclear accumulation due to their active transport along microtubules [5], thereby eliminating slow cytoplasmic transport from the cell periphery to the perinuclear region as a critical bottleneck to gene delivery for this system. An increasingly large fraction of gene vectors, however, became immobile over time in the perinuclear region of the cell, suggesting that the vectors may still face a formidable challenge in entering the nucleus. Particle tracking technology provides quantitative biophysical insights that are expected to guide the rational evolution of drug and gene vectors into more efficient systems.

In this review, results obtained with real-time MPT related to the transport of particulate drug carriers within intra- and extracellular barriers are summarized. Next, a brief synopsis of other biological applications of particle tracking is provided. Finally, key aspects of particle tracking technology are briefly reviewed. The reader is directed to other

publications for further details on particle tracking [9,10].

2. Intracellular barriers

Inefficient intracellular trafficking/transport of relatively large nonviral gene vectors has been suggested to be a critical barrier to efficient gene delivery [11–14]. Indeed, the molecularly crowded nature of the cytoplasm is known to hinder the transport of some macromolecules [15]. Investigations of the intracellular transport of nonviral gene vectors have mainly involved static methods, such as electron microscopy (EM) and fixed-cell confocal microscopy. Cytoplasmic transport, however, is a highly dynamic process which warrants the use of real-time, live-cell techniques. Real-time particle tracking has been recently used to quantify the transport of nonviral [5,6] and viral [16] gene vectors in live cells to reveal new insights into their intracellular transport.

2.1. Properties of cell cytoplasm

The cell cytoplasm is highly crowded by membrane-bounded compartments (organelles such as the endoplasmic reticulum (ER) and Golgi) and macromolecules (mostly proteins) [17,18]. Up to half of the cellular volume has been estimated to be comprised of membrane-bounded compartments [18] and the viscosity of the cytoplasm surrounding the organelles has been estimated to be similar to 12–13% Ficoll [19]. Actin microfilaments [20], intermediate filaments, and microtubules comprising the cytoskeleton also contribute to the heterogeneous intracellular milieu, posing steric obstacles to particle transport as well as binding surfaces for particles. Endogenous organelles exhibit sub-diffusive behavior (see Section 5.3 for discussion on transport modes) [18], relying on active transport mechanisms for efficient movement in cells. Active transport is mediated by cytoskeleton-dependent motor proteins such as myosin (actin-based), kinesin (microtubule-based), and dynein (microtubule-based). Dynein-mediated active transport, estimated to reach velocities of 0.7 $\mu\text{m/s}$ in vitro [21], would allow vesicles (or particles) to transport 10 μm in 14 s. More

comprehensive reviews of the cytoplasm [18] and active transport mechanism [22,23] can be found elsewhere.

2.2. Active transport of nonviral vectors

The intracellular transport of nonviral gene vectors was thought to be a potential bottleneck in gene delivery due to the highly crowded nature of the cytoplasm [11–14]. Live-cell MPT experiments, however, revealed that polyethylenimine (PEI)/DNA nanocomplexes are actively transported by motor proteins along microtubules [5] (Fig. 1A and B), a transport mechanism used by endogenous organelles [24], as well as by invading pathogens such as adenoviruses [25].

Actively transported gene vectors displayed transport rates much greater than nonactively transported vectors. At the short time scale of 33 ms, actively transported gene vectors displayed effective diffusivities (D_{eff}) similar to those not actively transported (see Section 5 for definitions of D_{eff} and time scale) [6]. At a longer time scale of 3 s, however, actively transported vectors exhibited a higher persistence of movement, with an average D_{eff} 30-fold greater than nonactively transported vectors. The average velocity of actively transported gene vectors was 0.2 $\mu\text{m/s}$ (Fig. 1C), a value including periods of saltatory motion, therefore underestimating the maximum achievable velocity. The trajectories of actively trans-

ported particles were along a linear/curvilinear path that often intersected the nucleus. Microtubule depolymerization with nocodazole decreased the percentage of actively transported nanocomplexes from 16% to 0% at 2 h posttransfection, suggesting the active transport of gene vectors occurs along microtubules.

2.3. Subdiffusive and immobile vectors

The majority (over 80%) of PEI/DNA nanocomplexes within cells displayed subdiffusive or immobile transport characteristics (see Section 5.3 for discussion on transport modes) and were primarily located in regions closest to the nucleus [5,6]. Interestingly, subdiffusive and immobile gene vectors exhibited two types of trajectories (Fig. 2), an apparently random motion (left of Fig. 2) and a “pearls-on-a-string” trajectory (right of Fig. 2). The “pearls-on-a-string” trajectory may be due to repeated binding and unbinding of gene vectors to microtubules or other intracellular structures. It is unclear, however, whether these gene vectors are inside (preescape) or outside (postescape) of endocytic vesicles.

Endosomes are known to have on–off kinetics with microtubules [26,27]; thus, it is likely that gene vectors within endosomes reflect the endosome transport properties. PEI/DNA nanocomplexes alone, however, displayed strong attraction to purified microtubules in an *in vitro* motility assay (unpub-

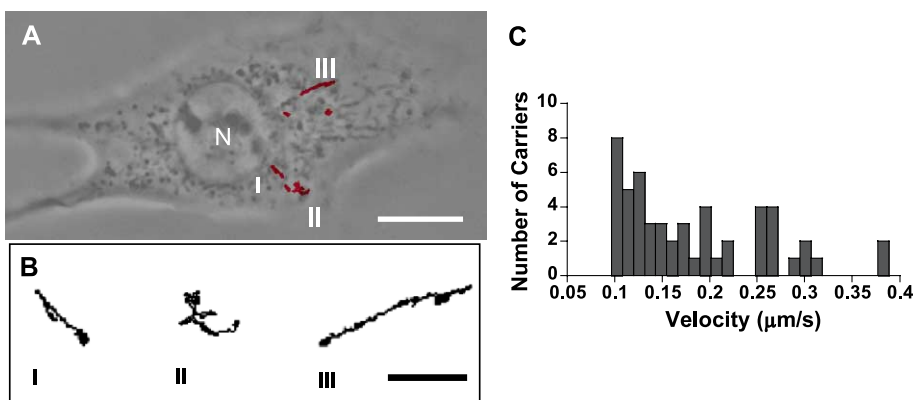


Fig. 1. Transport of intracellular PEI/DNA nanocomplexes. (A) Twenty-second trajectories (obtained at 33-ms intervals) of PEI/DNA complexes in a COS-7 cell 4 h posttransfection. Phase contrast image of the cell (obtained with a CCD camera) was overlaid with the trajectories of complexes. Three of six complexes shown displayed active transport with linear or curvilinear trajectories. Their detailed trajectories are shown in panel B. (C) Distribution of velocities of actively transported PEI nanocomplexes in COS-7 cells. For panel A, bar indicates 10 μm and N is nucleus. Bar in panel B is 2 μm . (Figures are from Refs. [5,6] with permission of the publishers.)

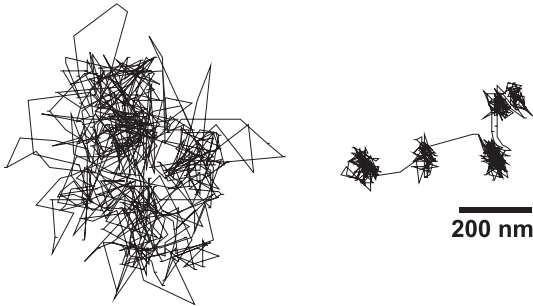


Fig. 2. Example trajectories of subdiffusive or immobile gene carriers. Each type of trajectory was seen for both immobile and subdiffusive transport modes. The gene carriers were tracked for 20 s at 33 ms intervals. (Figures are from Ref. [6] with permission of the publishers.)

lished observations), suggesting that gene vectors that have escaped endosomes may also associate with cytoskeletal elements to display the “pearls-on-a-string” trajectories. Therefore, an attraction of gene carriers, either inside or outside of endocytic vesicles, to cytoskeletal structures may account for subdiffusive and immobile transport modes being dominant near the cell nucleus. These results also suggest that gene vectors that have actively transported to the perinuclear region and have successfully escaped vesicles

may still face a formidable task in delivering their cargo into the nucleus.

2.4. Rapid perinuclear accumulation of gene vectors

The intracellular spatial distribution of PEI/DNA nanocomplexes was investigated by dividing the cytoplasm of each cell into four quadrants (Q1–Q4; Fig. 3A) [5]. PEI/DNA nanocomplexes accumulated in the perinuclear region (Q1) within 30 min (Fig. 3B). Approximately 40% of the gene vectors were found in the perinuclear quadrant Q1 at all time points (Fig. 3C shows 2 h posttransfection time point) [5]. Microtubule depolymerization with nocodazole inhibited the perinuclear accumulation of PEI/DNA nanocomplexes (Fig. 3C), suggesting that active transport along microtubules is required for rapid perinuclear accumulation of PEI/DNA gene vectors.

The physical transport of PEI/DNA nanocomplexes through the cell cytoplasm to the perinuclear region is not rate-limiting because the vectors are able to exploit the microtubule-based active transport mechanism, a strategy used by some of nature’s efficient DNA viruses [25]. Other bottlenecks to gene delivery in COS-7 cells must be considered, including

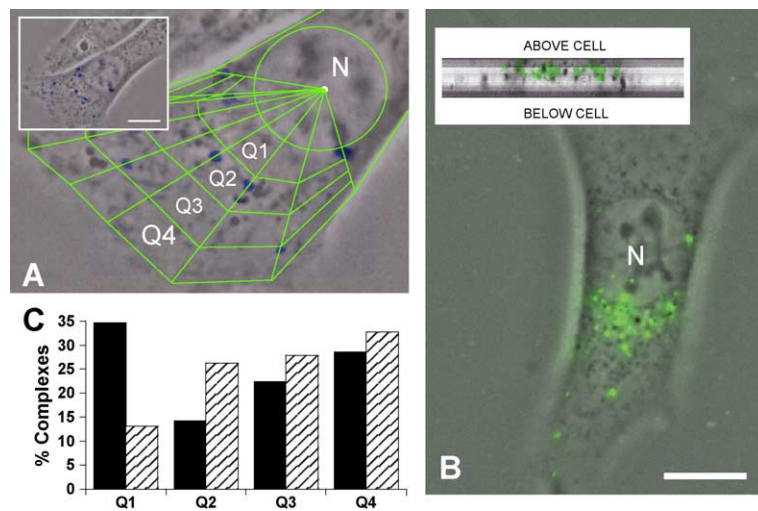


Fig. 3. Intracellular distribution of gene carriers. (A) The cytoplasm was divided into four quadrants (Q1–Q4). N indicates nucleus. Inset shows the cell without quadrants and with complexes in blue. Bar is 10 μ m. (B) A cell with gene vectors (green) accumulated in the perinuclear region. Inset shows the cross-section of the cell to demonstrate the complexes were intracellular. Bar is 10 μ m. For panels A and B, fluorescence images of the gene carriers are overlaid onto phase-contrast images obtained with a CCD camera. (C) Locations of complexes at 2 h posttransfection in cells with intact microtubules (solid black) and in nocodazole-treated cells (hatched). Note the lack of perinuclear accumulation in cells without intact microtubules. (Figures are from Ref. [5] with permission of the publishers.)

endosomal escape [28–30], nuclear import [31], and vector unpacking [32]. Our group is currently using MPT to investigate these other barriers.

3. Extracellular barriers

The mucus layer protecting epithelial surfaces of tissues is a critical extracellular barrier in drug and gene delivery, including the lungs (aerosol delivery) and the gastrointestinal tract (oral delivery). Multiple-particle tracking has recently been used to quantify particle transport rates in mucus and to gain insight into particle properties that can reduce adhesive interactions preventing rapid transport [2].

3.1. Particle transport in human cystic fibrosis (CF) mucus

Development of therapeutic gene delivery systems for cystic fibrosis (CF) has been difficult [1]. One cause of low transfection efficiency *in vivo* is inefficient transport rates of gene vectors in CF mucus, which acts as the primary extracellular barrier in the CF lung [33,34].

3.1.1. Properties of CF mucus

Mucin fibers in CF mucus, held together by disulfide bonds between mucin subunits and hydrogen bonds between the fibers, form a dense mesh that is intertwined by macromolecules such as filamentous actin and DNA [1]. The reduced liquid content and increased branching of mucus glycoproteins, along with the presence of neutrophil-derived DNA and cellular debris in CF mucus, leads to an increase in its viscoelasticity [35]. Mucus permeability is reduced as viscosity increases owing to increased viscous drag and steric obstruction from multiple mucus–particle interactions [36]. Small particles that avoid adhering to mucus should diffuse relatively rapidly, impeded only by viscous drag forces and the porous network of the mucus mesh [2,37].

3.1.2. Heterogeneous particle transport through CF mucus

The effect of drug/gene carrier size on transport rates through mucus obtained from patients with CF was investigated by tracking the motion of uniform

polystyrene particles of various diameters (100, 200, and 500 nm). Transport rates of the model drug carriers were heterogeneous to varying degrees in CF sputum (Fig. 4). The smallest particles (100 nm) exhibited the greatest range of transport rates, as quantified by mean-square displacement (MSD; Fig. 4A), which may be a reflection of their ability to access and move within pores formed by sputum components more readily than larger particles. Increasing the particle size led to more uniform transport properties (Fig. 4B and C), suggesting that larger particles are unable to transport through the vast majority of pores available to the smaller particles and are, thus, less affected by the microheterogeneity of CF sputum.

Interestingly, a small fraction of particles exhibited significantly greater transport rates than the majority. At a time scale of 100 ms, the fastest 10% of 100 nm particles contributed to ~80% of the ensemble MSD, whereas the fastest 10% of 200 nm particles contributed to ~60% of the ensemble (Fig. 4D). For 500 nm particles, the fastest 10% contributed to a little less than 40% of the ensemble value. In comparison, the fastest 10% of particles moving in a homogenous medium, such as glycerol, contribute to roughly 10% of the ensemble MSD. Therefore, larger particles (500 nm) displayed more homogeneous transport than smaller particles (100 and 200 nm). These results indicate that fast-moving “outlier” particles significantly affect ensemble average transport rates, an effect that was amplified as particle size decreased. Fast-moving “outlier” particles may be key for effective gene therapy for cystic fibrosis because it is estimated only 2–5% of lung epithelial cells must be transfected [38].

3.1.3. Micro- and macrorheology of CF mucus

The microviscosity of CF sputum was measured by particle tracking microrheology (see Section 5.4) and compared to the macroviscosity obtained with a strain-controlled cone and plate rheometer [2]. Smaller particles (100 nm) moved faster on average than slightly larger (200 nm) particles in CF sputum (Fig. 5A). At a time scale of 10s, the ensemble effective diffusivities of 100 and 200 nm particles in CF sputum were 1.5×10^{-2} and $4.5 \times 10^{-3} \mu\text{m}^2/\text{s}$, respectively. These diffusivity values show that the microviscosities, calculated from the Stokes–Einstein

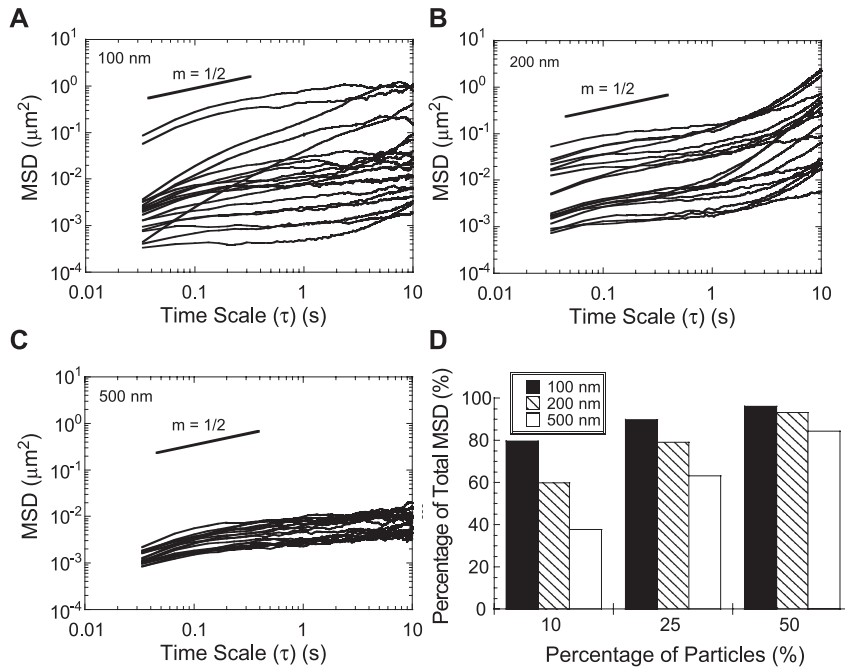


Fig. 4. Heterogeneities in particle transport rates in human CF sputum are reduced with increasing particle size. Individual MSDs of (A) 100, (B) 200, and (C) 500 nm particles. (D) The percentage contributions of the fastest 10%, 25%, and 50% particles to the ensemble mean-squared displacement ($\langle \text{MSD} \rangle$) is reduced with increasing particle size, confirming that the heterogeneity is reduced with increasing particle size. (Panels A–C are from Ref. [2] with permission of the publishers.)

equation (see Section 5.3.1), are 15- and 7- fold lower than the macroviscosity determined with the rheometer (Fig. 5B). In light of the observation that a small number of fast-moving particles strongly influence the average transport rates, this result indicates there may exist a small subpopulation of particles capable of

accessing pores in CF sputum filled with fluid that is significantly less viscous than the bulk viscosity of sputum. The microviscosity obtained with smaller 100 nm particles was lower than that of 200 nm particles, further evidence that smaller particles have greater access to pores in the CF sputum.

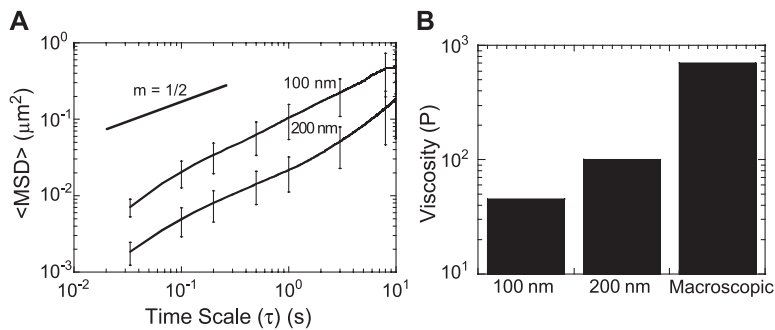


Fig. 5. Micro- and macrorheological properties of CF sputum. (A) Ensemble mean-squared displacements ($\langle \text{MSD} \rangle$) for 100- and 200-nm-diameter carboxylated polystyrene particles ($n \geq 100$ particles of each diameter) in CF sputum ($n=3$ mucus samples). (B) CF mucus microviscosities determined with particle tracking (calculated from $\langle \text{MSD} \rangle$ at $\tau=10$ s, equivalent to shear rate of 0.1 s^{-1} , for 100 or 200 nm particles), and macroviscosity determined with cone and plate rheometer (shear rate of 0.1 s^{-1}). (Figures are adapted from Ref. [2] with permission of the publishers.)

3.1.4. Effects of mucolytic agents

An improved understanding of the relationship between CF mucus properties, which can be manipulated by mucolytic agents currently used to reduce the viscosity of CF mucus [39], and particle transport is critical to the design of DNA carriers for delivery in the nondistal airways of the lungs [40]. Treatment of CF sputum with rhDNase (Pulmozyme®) reduces mucus viscosity by hydrolyzing chromosomal DNA released from dead neutrophils [41].

Interestingly, treatment with rhDNase did not change the ensemble MSD of 200 nm particles in human CF mucus (Fig. 6A). Treatment with the mucolytic agent did, however, decrease the heterogeneity of particle transport rates through CF sputum (Fig. 6B and C). Consistent with these observations is the hypothesis that the fastest moving particles present in the no treatment case may be slowed upon DNase treatment due to the increased microviscosity of the medium in the pores (caused by the diffusion of cleaved DNA fragments into the fluid-filled pores). The slowest moving particles present prior to DNase treatment may, upon treatment, be released from highly constricting environments and, therefore, display increased transport rates.

3.2. Particle transport in gastrointestinal mucus

The gastrointestinal (GI) tract is also lined with a protective mucus barrier that may limit effective particulate-based drug/gene delivery. The transport of cationic nanoparticles through gastric mucus was quantified with particle tracking and compared to

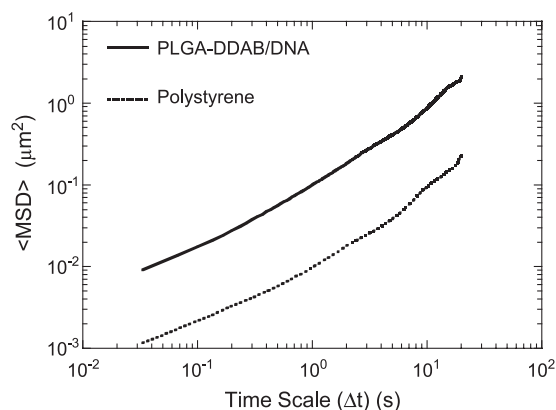


Fig. 7. Ensemble MSD of similarly sized PLGA-DDAB/DNA and 200 nm carboxylated polystyrene nanoparticles in pig gastric mucus. (From Ref. [3].)

similarly sized polystyrene particles [3]. The cationic nanoparticles were composed of poly(lactic-co-glycolic) acid (PLGA) and the cationic surfactant, dimethyldioctadecyl ammonium bromide (DDAB), to which DNA was condensed on the particle surface.

Remarkably, PLGA-DDAB/DNA nanoparticles displayed 10-fold greater ensemble MSD than polystyrene particles of similar size (Fig. 7), making them promising drug/gene carriers for delivery through mucus. By analyzing the transport behavior of hundreds of individual particles with multiple particle tracking, it was determined that 93% of polystyrene particles experienced restricted subdiffusive transport in GI mucus, whereas only 78% of PLGA-DDAB/DNA nanoparticles were restricted. This difference may be due to reduced PLGA-DDAB/DNA particle adhesion to mucus compared to polystyrene particles.

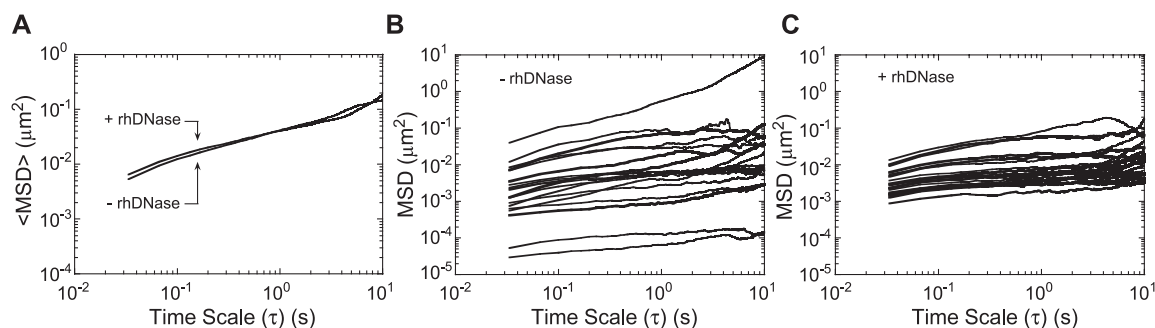


Fig. 6. Transport of nanoparticles in human CF sputum treated with rhDNase. (A) Effect of rhDNase treatment (7 $\mu\text{g}/\text{ml}$, 30 min) on the ensemble MSD of 200 nm polystyrene particles in CF sputum. Individual MSDs of particles in CF mucus with (B) no treatment and (C) after rhDNase treatment. The heterogeneities in particle MSD are reduced with rhDNase treatment of CF mucus. (Figures are from Ref. [2] with permission of the publishers.)

Investigations are underway to understand the physicochemical properties responsible for the enhanced particle transport and to further reduce particle interactions with mucus.

4. Other applications

Particle tracking is a useful method to characterize the transport of proteins and colloids (e.g., drug/gene carriers) in complex fluids with high spatio-temporal resolution. Other biological applications include characterizing the viscoelasticity of the cell cytoplasm, quantifying the motion of plasma membrane components, and investigating the infection pathway of viruses.

4.1. Viral gene delivery vectors

Adeno-associated viruses (AAV), often used for gene therapy applications, were labeled with single-dye molecules and tracked in real time to reveal biophysical insights into their infection pathway [42]. AAV free of endosomes displayed average diffusivities twofold greater than those still inside vesicles. Actively transported AAV exhibited velocities between 1.8 and 3.7 $\mu\text{m/s}$, which are on the same order of magnitude as dynein-mediated active transport [24]. Active transport of AAV was dependent on the presence of intact microtubules.

4.2. Characterizing cell cytoplasm

As models of the cell cytoplasm, viscoelastic properties of actin solutions have been characterized by tracking the motion of beads embedded in the gel [8,43]. Actin gels were found to be highly heterogeneous, especially in the presence of actin-bundling proteins such as fascin [43]. Such descriptions of the cell cytoplasm have important consequences in biochemistry [18] where intracellular enzymes were once thought to be in homogeneous environments. Heterogeneity in the cytoplasm may cause enzymes to be segregated and concentrated in certain regions, thereby making intracellular reactions spatially dependent.

Recently, the motion of beads microinjected directly into the cytoplasm were tracked to ascertain

the viscoelastic properties of the cytoplasm in intact cells [7]. The compliance of the cell cytoarchitecture appears to depend on the relative distance to the cell nucleus, with the region closest to the nucleus being mechanically the softest.

4.3. Motion of plasma membrane components

An active area of research involving particle tracking technology is the study of the motion of plasma membrane components [10,44–48]. Using gold-labeled antibodies specific for the components, or fluorescently tagged components themselves, researchers have quantitatively characterized the motion of phospholipids [44,45] and transmembrane proteins [10,46,47]. Fujiwara et al. [45] showed phospholipids in the cell membrane undergo hop diffusion between compartments formed by transmembrane proteins anchored to the underlying actin cytoskeleton. Class I major histocompatibility complex molecules (MHC I) also experienced confined diffusion on the surface of cells, and a deficiency in α -spectrin (a protein involved in the formation of the underlying cytoskeleton along with actin) almost doubled the confined area from 330 to 650 nm [47], further defining the role of the cytoskeleton in the mobility of plasma membrane components. Such particle tracking studies are helping to revise our understanding of plasma membrane structure, and how it contributes to important cellular functions such as cell signaling.

5. Particle tracking technology: a brief tutorial

Single-particle tracking (SPT) has been used in the field of membrane dynamics to uncover the transport behavior of proteins and lipids associated with the plasma membrane [10,44–47]. MPT was subsequently developed as a high throughput version of SPT and has been used to deduce the viscoelastic properties of complex fluids such as actin solutions [8,43] and the intracellular environment [7]. This section briefly discusses the basics of high-resolution particle tracking. Readers are referred to Table 1 for a list of symbols and abbreviations used in the equations and text in the following sections.

Table 1
Listing of symbols and abbreviations used in the equations in this review

Symbol	Parameter	Definition
τ	time scale	unit of time over which particle displacement is calculated
$\Delta x, \Delta y$ or Δz	displacement	particle displacement in the x, y or z direction
MSD or $\langle \Delta r^2(\tau) \rangle$	mean-square displacement	time-dependent displacement of a particle, squared
$\langle \text{MSD} \rangle$ or $\langle \langle \Delta r^2(\tau) \rangle \rangle$	ensemble mean-square displacement	average of individual particle MSDs
D_0	time-independent diffusivity	diffusivity of a particle undergoing simple diffusion
D_{eff} or $D(\tau)$	effective diffusivity or time-dependent diffusivity	diffusivity of a particle without regard to mode of transport
$\langle D_{\text{eff}} \rangle$	ensemble effective diffusivity	average of individual particle effective diffusivities
v	velocity	mean velocity of a particle undergoing active or convective motion
α	anomalous exponent (value less than 1)	characterizes anomalous, or sub-diffusive, particle transport

5.1. Time scale

The concept of time scale may not be intuitive at first, but its importance to particle tracking necessitates its discussion. The shortest time scale achievable for a given experimental setup is determined by the maximum speed of the camera and the necessary acquisition hardware. Assuming a camera is able to capture images at video rate, or 30 frames/s, the shortest time scale is 33 ms. The longest time scale, of course, depends on the length of the movie.

To illustrate the use of time scale, assume a 20-s movie was captured at 30 frames/s, resulting in a total of 600 frames recording the movement of a particle. The time interval between each frame is 33 ms (Fig. 8); therefore, the change in particle displacement from frame-to-frame can be calculated. A movie of 600 frames results in 599 displacement values. Squaring the 599 displacements and determining the mean value results in the mean-square displacement (MSD) at the time scale of 33 ms. The next shortest time scale is 66 ms (Fig. 8), and there are 598 displacement values for this time scale. At the other extreme, the largest time scale for this example is 19,967 ms (20 s minus 33 ms), with one displacement value. Thus, time scale is the time over which a particle is allowed to move before calculating its displacement from an initial point. Because the particle is given more time to move for longer time scales, it is logical to expect that the MSD value will increase with increasing time scale.

By examining MSD values over time scale, insightful information on particle transport can be obtained. For example, changes in the slope of the MSD with respect to time scale can be used to

characterize the local dynamics of the microenvironment surrounding each probe particle. In gels or porous networks with small mesh sizes, micron-sized particles may undergo subdiffusive transport at short time scales; however, at larger time scales, particle motion may appear more diffusive (see Section 5.3 for discussion on transport modes). The switch from subdiffusive to diffusive transport may indicate (a) transient binding of the particles to molecular partners or (b) the presence of soft dynamic obstacles created by the gel microstructure, which promote entropic caging of the particles and prevent their “free” viscous diffusion. The apparent free viscous diffusion at longer time scales suggests untrapping of the particle due to desorption and/or relaxation of polymer structures (e.g., mucus fibers, actin filaments) surrounding the particle. These two different time-scale regimes can be intuitively understood as follows. When tracked with a fast camera (i.e., short time scales, high frequencies), particles in a partially elastic medium may appear trapped in local cages, and the fluid behaves like an elastic solid. When tracked with a slow camera (i.e., long time

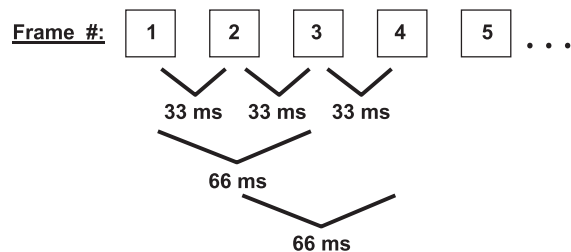


Fig. 8. Illustration of time scale for a movie obtained at 30 frames/s.

scales, low frequencies), the particles move from “cage to cage” because the fluid has had sufficient time to relax, and the fluid behaves as a viscous liquid. This characteristic switch from subdiffusive to diffusive transport, or the uncaging effect, has been observed in colloidal suspensions near the glass transition temperature [49] and in CF sputum [2].

5.2. Individual vs. ensemble transport properties

Given x and y positional data of the transporting particles over time, the mean-square displacement, MSD or $\langle \Delta r^2(\tau) \rangle$, in two dimensions, x and y , of each particle (Fig. 9A) is

$$\langle \Delta r^2(\tau) \rangle = \langle \Delta x^2 + \Delta y^2 \rangle. \quad (1)$$

See Section 5.5 for discussion on tracking in two versus three dimensions. Effective diffusivities (D_{eff}); (Fig. 9B) can then be obtained by

$$D_{\text{eff}} = \langle \Delta r^2(\tau) \rangle / (4\tau). \quad (2)$$

The ability to capture the transport behavior of hundreds of carriers at the single-particle level is an advantage over purely ensemble techniques such as fluorescence recovery after photobleaching (FRAP). With particle tracking, particles can be classified into subpopulations to yield insightful information such as transport mode (active, diffusive, subdiffusive), trajectory, and directionality [5]. MSD or D_{eff} values for individual particles can then be averaged to

obtain ensemble values, as indicated by $\langle \text{MSD} \rangle$ or $\langle D_{\text{eff}} \rangle$ (Fig. 9C). Therefore, particle tracking allows the investigation of particle transport on the level of large populations and as individual entities.

5.3. Transport modes

Particle transport rates in complex environments, such as the cell cytoplasm, are heterogeneous. For example, following cell entry, nonviral gene vectors were transported in COS-7 cells at various rates [5], with some vectors moving several orders of magnitude faster than others. In contrast, transport of polystyrene beads in glycerol is homogeneous (all particles moving by simple diffusion). Heterogeneity of particle transport has also been observed in extracellular environments, such as mucus (see Section 3.1.2).

Because particle tracking allows single-particle resolution, similarly transporting particles can be grouped into useful classes, such as transport modes, that provide important insights into particle transport mechanisms and limitations. Graphing the effective diffusivity (D_{eff}) of individual particles versus τ (Fig. 10) is one way to determine the mode of particle transport [47,50]. A particle displaying a constant D_{eff} with respect to τ suggests it is undergoing simple diffusion (thermally driven Brownian motion). Actively transported particles display a D_{eff} that increases with τ and subdiffusive particles display a D_{eff} that decreases with τ . MSD versus τ curves representing the three transport modes can be found in Ref. [5]. More in depth discussion on

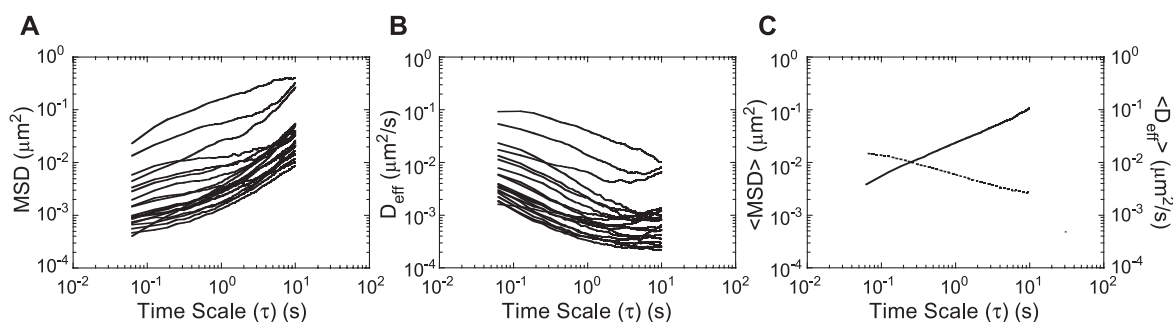


Fig. 9. Particle tracking allows characterization of (A, B) individual particle transport rates and (C) ensemble-averaged bulk properties. Transport rates of 200 nm polystyrene particles in human cystic fibrosis (CF) sputum treated with 65 $\mu\text{g/ml}$ *N*-acetylcysteine. (A) Individual MSDs of 20 randomly selected particles and (B) of individual time-dependent effective diffusivities (D_{eff}). Each line in panels A and B represent the data for a single particle. (C) Ensemble MSD ($\langle \text{MSD} \rangle$) (solid) and ensemble D_{eff} ($\langle D_{\text{eff}} \rangle$) (dashed).

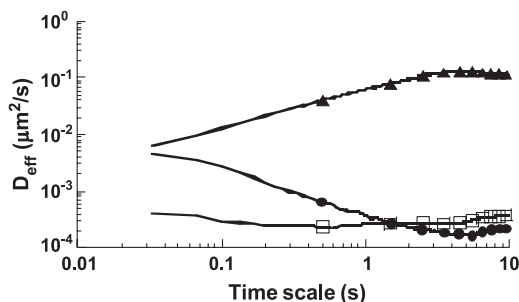


Fig. 10. Different transport modes of drug and gene carriers. Transport modes of gene carriers are classified into three groups based on their characteristic D_{eff} curves: diffusive (\square), subdiffusive (\bullet), and active (\blacktriangle). The markers of only ten data points per gene carrier are shown to distinguish the curves. The PEI/DNA nanocomplexes previously classified as diffusive are now more usefully classified as the immobile fraction (see Section 5.3.5). (Figures are from Ref. [6] with permission of the publishers.)

transport mode characterization can be found elsewhere [9,10].

5.3.1. Simple diffusion

The MSD, or $\langle \Delta r^2(\tau) \rangle$, of particles undergoing simple diffusion is given by

$$\langle \Delta r^2(\tau) \rangle = 4D_0\tau, \quad (3)$$

where D_0 is the diffusion coefficient independent of time scale (τ). D_0 can be obtained by fitting the MSD vs. τ curve to a linear function. In this case, the Stokes–Einstein relation,

$$D_0 = k_B T / 6\pi\eta a \quad (4)$$

(where k_B is Boltzmann’s constant, T is temperature in Kelvin, η is fluid viscosity and a is particle radius), applies to the transporting particles. The experimental diffusivity obtained through particle tracking can be used to determine the viscosity of the medium through which particles are transporting (see Section 3.1.3) [2].

To categorize particles as undergoing simple diffusion, they should fit the mathematical criteria (see above) as well as other appropriate criteria relevant to the system under study, such as characteristic trajectory and the relative diffusivity values (see Section 5.3.5 for discussion on these criteria). Particles not meeting these criteria may more usefully be classified into a different transport mode, such as the immobile fraction (see Section 5.3.5).

5.3.2. Anomalous subdiffusive transport

Subdiffusive transport, or anomalous diffusion [9,50], can be described by

$$\langle \Delta r^2(\tau) \rangle = 4D\tau^\alpha \quad (5)$$

where D is the diffusion coefficient and α is the anomalous exponent equal to less than 1. This transport mode can be due to the motion of particles impeded by obstacles [50], or by particle binding to physical structures in the environment [51].

5.3.3. Corralled motion

Researchers investigating lipid membrane domains are interested in a type of nonnormal diffusion termed corralled motion, where particle transport is confined to corals for periods of time before jumping to the next coral [9,45]. Given the particle size, and by calculating particle displacements within transient confinement zones (TCZ) [52], the radius of pores or confinement areas through which particles are transporting can be determined.

5.3.4. Active transport

The motion of actively transported particles is described by

$$\langle \Delta r^2(\tau) \rangle = 4D_0\tau + v^2\tau^2 \quad (6)$$

where v is the mean nanocomplex velocity. The values of D_0 and v can be obtained by fitting the MSD vs. τ curve to a polynomial. In systems without active transport mechanisms, the added term characterizes convection, perhaps due to fluid flow.

5.3.5. Immobile

Using the purely mathematical criteria set forth in previous sections, particles may be classified as moving by simple diffusion, but may be more usefully classified as immobile [6,10]. For example, polyethylenimine (PEI)/DNA nanocomplexes classified as moving by simple diffusion within cells [5] displayed average diffusivity values equal to or less than that of subdiffusive complexes at most time scales (Fig. 11). This is counterintuitive because subdiffusive particles are expected to move at rates less than particles moving by simple diffusion in cells. Additionally, many of the “diffusive” particles exhibited “pearls-on-a-string” trajectories (see Section 2.3) that are not characteristic of

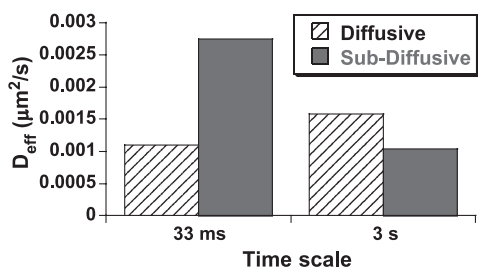


Fig. 11. Effective diffusivity (D_{eff}) of diffusive and subdiffusive gene carriers in live cells at short (33 ms) and long (3 s) time scales. Kruskal–Wallis test determined the D_{eff} values for diffusive carriers are similar at the two time scales, whereas the difference between D_{eff} values for subdiffusive carriers are statistically significant ($p < 10^{-5}$) at the two different time scales. These “diffusive” carriers are now more accurately referred to as “immobile”. The difference between diffusive and subdiffusive carriers at the longer time scale of 3 s is not statistically significant. (Figures are from Ref. [6] with permission of the publishers.)

simple diffusion, thereby making transport mode categorization dependent not only on mathematical criteria, but also on qualitative observations. Immobile gene vectors may be adhered to cytoskeletal elements (thus their movements may appear Brownian, but may merely reflect the thermal vibration of the cytoskeleton), or may be trapped in tight cages formed by cellular components, including the cytoskeleton.

5.4. Diffusivities

Particle transport in complex environments may be described with three different diffusivities: microscopic, mesoscopic, and macroscopic diffusion coefficients.

5.4.1. Microscopic diffusion

Nanoparticles diffusing in complex biological fluids may move in microdomains or pores that contain a lower viscosity fluid than measured by bulk-fluid

rheological characterization [2]. Multiple-particle tracking can be used to probe the viscosity in these microdomains provided that particles are nonadhesive and small enough to move freely in the interstitial fluid (Fig. 12A). In these cases, the Stokes–Einstein equation (see Section 5.3.1) is used to calculate the microviscosity [2]. Because this equation assumes that particles are moving by simple diffusion, the microscopic diffusivity is calculated from the MSD at early time scales when particles undergo unhindered short range Brownian motion [10]. The validity of this assumption depends on the combination of experimental system (e.g., proteins v. larger colloids; fluid properties) and the experimental setup (e.g., speed of camera). For example, a colloid similar in size to the pore within which it is moving may require a very fast camera to capture purely diffusive transport since the colloid comes into contact with the pore boundaries quickly, whereas a smaller protein in the same pore may appear purely diffusive even without the faster camera. The microscopic diffusivity of the particle can also be extrapolated to longer time scales, and this “theoretical” curve can then be used to pose criteria on assigning transport modes [10].

5.4.2. Mesoscopic diffusion

When the diameter of tracked particles approaches the size of the fluid pores in complex environments, particle transport is greatly affected by dynamics of the fluid microstructure (Fig. 12B). In this region of mesoscopic transport, the particle motion at early time scales may appear hindered (caged motion); however, at longer time scales changes in the microstructure of the fluid can lead to the appearance of diffusive motion. Particles undergoing this anomalous diffusion often display biphasic behavior, where D_{eff} decreases with τ at short time scales and approaches a constant

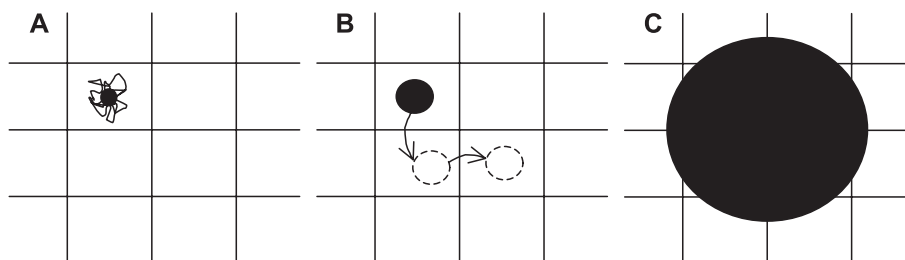


Fig. 12. Three important length scales of transport in complex environments: (A) microscopic, (B) mesoscopic, and (C) macroscopic.

value at long time scales [50]. This constant lower value reflects the mesoscopic diffusion coefficient. A viscosity calculated from the mesoscopic diffusivity (termed microviscosity in Ref. [2]) may be lower than the viscosity measured by traditional rheological techniques (termed macroviscosity) because the particles have access to the lower viscosity pores and, therefore, have greater freedom in motion. By tracking particles undergoing mesoscopic transport, the local environments in heterogeneous solutions (such as mucus) can be probed and information such as pore size can be obtained [2,8,53].

5.4.3. Macroscopic diffusion

Multiple-particle tracking can be used to determine the bulk-fluid rheological properties with the accuracy of traditional techniques, such as strain-controlled cone and plate rheometry [7,54]. To accurately probe the bulk fluid properties, the diameter of particles should be significantly larger than the fluid pore sizes (thus the fluid appears as a homogeneous solution to the particles; Fig. 12C). The key advantage of particle tracking over traditional methods is the requirement of substantially less sample volume. For example, a cone and plate rheometer typically requires >1 ml of sample, whereas particle tracking in our lab has been accomplished reproducibly with ~10 μ l of mucus sample.

5.5. 2D v. 3D tracking

As stated previously, the mean-square displacement (MSD) in two dimensions, x and y , is given by

$$\text{MSD} = \langle \Delta r^2(\tau) \rangle_{2D} = \langle \Delta x^2 + \Delta y^2 \rangle. \quad (1)$$

By assuming the medium through which the particles transport is locally isotropic, particle displacements in the x , y , and z axes can be assumed to be uncorrelated. In another words,

$$\begin{aligned} \langle \Delta r^2(\tau) \rangle_{2D} &= \langle \Delta x^2 \rangle + \langle \Delta y^2 \rangle \\ &= (2/3)[\langle \Delta x^2 \rangle + \langle \Delta y^2 \rangle + \langle \Delta z^2 \rangle] \\ &= (2/3)\langle \Delta r^2(\tau) \rangle_{3D}. \end{aligned}$$

The end result is that the two-dimensional (2D) diffusion coefficient is equal to the three-dimensional (3D) diffusion coefficient (as well as equal to the one-dimensional (1D) diffusion coefficient) in isotropic environments.

This assumption may not be valid in environments characterized by structures highly ordered in one direction and depends on the length scales involved. To illustrate the importance of length scales, Fig. 13 shows two differently sized particles moving by diffusion in two dimensions in an environment characterized by filaments highly ordered in the x -direction. When particle diameter is much less than the pore diameter, particle transport in the x and y directions will be similar, or $\langle \Delta x^2 \rangle = \langle \Delta y^2 \rangle$. In this example, however, when particle diameter is on the same order of magnitude as the pore diameter, transport in the y direction will clearly be less than transport in the x direction, or $\langle \Delta x^2 \rangle \neq \langle \Delta y^2 \rangle$. Thus, environments with ordered structures can be locally isotropic depending on the length scales involved.

If the isotropic assumption fails for a specific system under study, three-dimensional transport properties can be experimentally determined by using changes in fluorescence intensity as a measure of movement in the axial z -direction [55]. Microscopes equipped with a motorized z -drive can be used to track the motion of particles in all three axes (x , y , and z); however, particle movements may be too rapid in certain systems to accurately capture their three-dimensional motion.

5.6. Tracking resolution

With particle tracking, the transport of individual particles can be obtained with resolutions smaller than the wavelength of light [56]. Tracking resolution (the

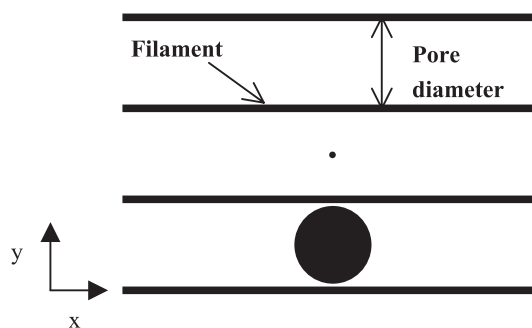


Fig. 13. The size of particle relative to the pore diameter, created by highly ordered filaments in one direction, is an important parameter in assessing the validity of the isotropic assumption. If filaments are randomly or equally ordered in all directions, the isotropic assumption will hold even if particle size approaches that of the pore diameter.

ability to track the light-intensity-weighted centroid of diffraction-limited images) is different from spatial resolution (the ability to resolve two separate entities) and can be obtained by two methods. The first method involves tracking the motion of particles firmly adhered to a coverslip, and has been reported to be around 5 nm [43]. Thus, the tracking resolution is better than the spatial resolution of a system. Alternatively, the particle tracking resolution can be determined by fitting the MSD of particles moving by simple diffusion (e.g., polystyrene beads moving in glycerol) to

$$\langle \Delta r^2(\tau) \rangle = 4\sigma^2 + 4D_0\tau \quad (7)$$

where σ is the resolution [57].

6. Conclusions

Real-time multiple particle tracking is a high-resolution technology useful for quantifying the transport of individual drug and gene carriers in complex biological barriers, such as the cell cytoplasm or mucus lining the GI tract or the airways of the lungs. Studies with particle tracking provide novel insights into the interactions and processes involved in the transport of drug and gene vectors through these important barriers and promises to aid in the rational evolution of therapeutic colloids.

References

- [1] J. Hanes, M. Dawson, Y. Harel, J. Suh, J. Fiegel, in: A.J. Hickey (Ed.), *Gene Delivery to the Lung*, in *Pharmaceutical Inhalation Aerosol Technology*, Marcel Dekker, New York, 2003, pp. 489–539.
- [2] M. Dawson, D. Wirtz, J. Hanes, Enhanced viscoelasticity of human cystic fibrotic sputum correlates with increasing microheterogeneity in particle transport, *J. Biol. Chem.* 278 (2003) 50393–50401.
- [3] M. Dawson, E. Krauland, D. Wirtz, J. Hanes, Transport of polymeric nanoparticle gene carriers in gastric mucus, *Biotechnol. Prog.* 20 (2004) 851–857.
- [4] C. Kitson, B. Angel, D. Judd, S. Rothery, N.J. Severs, A. Dewar, L. Huang, S.C. Wadsworth, S.H. Cheng, D.M. Geddes, E.W. Alton, The extra- and intracellular barriers to lipid and adenovirus-mediated pulmonary gene transfer in native sheep airway epithelium, *Gene Ther.* 6 (1999) 534–546.
- [5] J. Suh, D. Wirtz, J. Hanes, Efficient active transport of gene nanocarriers to the cell nucleus, *Proc. Natl. Acad. Sci. U. S. A.* 100 (2003) 3878–3882.
- [6] J. Suh, D. Wirtz, J. Hanes, Real-time intracellular transport of gene nanocarriers studied by multiple particle tracking, *Biotechnol. Prog.* 20 (2004) 598–602.
- [7] Y. Tseng, T.P. Kole, D. Wirtz, Micromechanical mapping of live cells by multiple-particle-tracking microrheology, *Biophys. J.* 83 (2002) 3162–3176.
- [8] M.T. Valentine, P.D. Kaplan, D. Thota, J.C. Crocker, T. Gisler, R.K. Prud'homme, M. Beck, D.A. Weitz, Investigating the microenvironments of inhomogeneous soft materials with multiple particle tracking, *Phys. Rev., E Stat. Nonlinear Soft Matter Phys.* 64 (2001) 061506.
- [9] M.J. Saxton, K. Jacobson, Single-particle tracking: applications to membrane dynamics, *Annu. Rev. Biophys. Biomol. Struct.* 26 (1997) 373–399.
- [10] A. Kusumi, Y. Sako, M. Yamamoto, Confined lateral diffusion of membrane receptors as studied by single particle tracking (nanovid microscopy). Effects of calcium-induced differentiation in cultured epithelial cells, *Biophys. J.* 65 (1993) 2021–2040.
- [11] D. Luo, W.M. Saltzman, Synthetic DNA delivery systems, *Nat. Biotechnol.* 18 (2000) 33–37.
- [12] C.W. Pouton, L.W. Seymour, Key issues in non-viral gene delivery, *Adv. Drug Deliv. Rev.* 46 (2001) 187–203.
- [13] R. Kircheis, L. Wightman, E. Wagner, Design and gene delivery activity of modified polyethylenimines, *Adv. Drug Deliv. Rev.* 53 (2001) 341–358.
- [14] G.L. Lukacs, P. Haggie, O. Seksek, D. Lechardeur, N. Freedman, A.S. Verkman, Size-dependent DNA mobility in cytoplasm and nucleus, *J. Biol. Chem.* 275 (2000) 1625–1629.
- [15] K. Luby-Phelps, P.E. Castle, D.L. Taylor, F. Lanni, Hindered diffusion of inert tracer particles in the cytoplasm of mouse 3T3 cells, *Proc. Natl. Acad. Sci. U. S. A.* 84 (1987) 4910–4913.
- [16] J.S. Suk, J. Suh, J. Hanes, Cellular uptake and intracellular transport of viral and non-viral gene vectors in differentiated neurons affected in Parkinson's disease, *Proc. Am. Inst. Chem. Eng.* 2004, (in press).
- [17] R.J. Ellis, Macromolecular crowding: obvious but underappreciated, *Trends Biochem. Sci.* 26 (2001) 597–604.
- [18] K. Luby-Phelps, Cytoarchitecture and physical properties of cytoplasm: volume, viscosity, diffusion, intracellular surface area, *Int. Rev. Cytol.* 192 (2000) 189–221.
- [19] L. Hou, F. Lanni, K. Luby-Phelps, Tracer diffusion in F-actin and Ficoll mixtures. Toward a model for cytoplasm, *Biophys. J.* 58 (1990) 31–43.
- [20] T. Ito, A. Suzuki, T.P. Stossel, Regulation of water-flow by actin-binding protein-induced actin gelation, *Biophys. J.* 61 (1992) 1301–1305.
- [21] S.J. King, T.A. Schroer, Dynactin increases the processivity of the cytoplasmic dynein motor, *Nat. Cell Biol.* 2 (2000) 20–24.
- [22] S.F. Hamm-Alvarez, Molecular motors and their role in membrane traffic, *Adv. Drug Deliv. Rev.* 29 (1998) 229–242.
- [23] T.A. Schroer, Motors, clutches and brakes for membrane traffic: a commemorative review in honor of Thomas Kreis, *Traffic* 1 (2000) 3–10.

- [24] H. Lodish, A. Berk, S.L. Zipursky, P. Matsudaira, D. Baltimore, J. Darnell, *Molecular Cell Biology*, 3rd ed., W. H. Freeman, New York, 1995, pp. 1070–1078.
- [25] P.L. Leopold, G. Kreitzer, N. Miyazawa, S. Rempel, K.K. Pfister, E. Rodriguez-Boulant, R.G. Crystal, Dynein- and microtubule-mediated translocation of adenovirus serotype 5 occurs after endosomal lysis, *Hum. Gene Ther.* 11 (2000) 151–165.
- [26] M. Clarke, J. Kohler, J. Heuser, G. Gerisch, Endosome fusion and microtubule-based dynamics in the early endocytic pathway of *Dictyostelium*, *Traffic* 3 (2002) 791–800.
- [27] S.J. King, C.L. Brown, K.C. Maier, N.J. Quintyne, T.A. Schroer, Analysis of the dynein–dynactin interaction in vitro and in vivo, *Mol. Biol. Cell* 14 (2003) 5089–5097.
- [28] C. Plank, B. Oberhauser, K. Mechtler, C. Koch, E. Wagner, The influence of endosome-disruptive peptides on gene transfer using synthetic virus-like gene transfer systems, *J. Biol. Chem.* 269 (1994) 12918–12924.
- [29] D.W. Pack, D. Putnam, R. Langer, Design of imidazole-containing endosomolytic biopolymers for gene delivery, *Biotechnol. Bioeng.* 67 (2000) 217–223.
- [30] M. Ogris, R.C. Carlisle, T. Bettinger, L.W. Seymour, Melittin enables efficient vesicular escape and enhanced nuclear access of nonviral gene delivery vectors, *J. Biol. Chem.* 276 (2001) 47550–47555.
- [31] J.A. Wolff, M.G. Sebestyen, Nuclear security breached, *Nat. Biotechnol.* 19 (2001) 1118–1120.
- [32] D.V. Schaffer, N.A. Fidelman, N. Dan, D.A. Lauffenburger, Vector unpacking as a potential barrier for receptor-mediated polyplex gene delivery, *Biotechnol. Bioeng.* 67 (2000) 598–606.
- [33] S. Ferrari, C. Kitson, R. Farley, R. Steel, C. Marriott, D.A. Parkins, M. Scarpa, B. Wainwright, M.J. Evans, W.H. Colledge, D.M. Geddes, E.W. Alton, Mucus altering agents as adjuncts for nonviral gene transfer to airway epithelium, *Gene Ther.* 8 (2001) 1380–1386.
- [34] C. Kitson, B. Angel, D. Judd, S. Rothery, N.J. Severs, A. Dewar, L. Huang, S.C. Wadsworth, S.H. Cheng, D.M. Geddes, E.W.F.W. Alton, The extra- and intracellular barriers to lipid and adenovirus-mediated pulmonary gene transfer in native sheep airway epithelium, *Gene Ther.* 6 (1999) 534–546.
- [35] P.G. Bhat, D.R. Flanagan, M.D. Donovan, Drug diffusion through cystic fibrotic mucus: steady-state permeation, rheologic properties, and glycoprotein morphology, *J. Pharm. Sci.* 85 (1996) 624–630.
- [36] R.A. Cone, Mucus, in: P.L. Ogra (Ed.), *Mucosal Immunology*, Academic Press, San Diego, CA, 1999, pp. 43–64.
- [37] N.N. Sanders, S.C. De Smedt, E. Van Rompaey, P. Simoens, F. De Baets, J. Demeester, Cystic fibrosis sputum: a barrier to the transport of nanospheres, *Am. J. Respir. Crit. Care Med.* 162 (2000) 1905–1911.
- [38] D. Geddes, E. Alton, Cystic fibrosis clinical trials, *Adv. Drug Deliv. Rev.* 30 (1998) 205–217.
- [39] J.M. Zahm, C. Debordeaux, C. Maurer, D. Hubert, D. Dusser, N. Bonnet, R.A. Lazarus, E. Puchelle, Improved activity of an actin-resistant DNase I variant on the cystic fibrosis airway secretions, *Am. J. Respir. Crit. Care Med.* 163 (2001) 1153–1157.
- [40] M. Fuloria, B.K. Rubin, Evaluating the efficacy of mucoactive aerosol therapy, *Respir. Care* 45 (2000) 868–873.
- [41] R. Mersny, A. Daugherty, S. Short, R. Widmer, M. Siegel, G. Keller, Distribution of DNA and alginate in purulent cystic fibrosis sputum: implications to pulmonary targeting strategies, *J. Drug Target.* 4 (1996) 233–243.
- [42] G. Seisenberger, M.U. Ried, T. Endress, H. Buning, M. Hallek, C. Brauchle, Real-time single-molecule imaging of the infection pathway of an adeno-associated virus, *Science* 294 (2001) 1929–1932.
- [43] J. Apgar, Y. Tseng, E. Fedorov, M.B. Herwig, S.C. Almo, D. Wirtz, Multiple-particle tracking measurements of heterogeneities in solutions of actin filaments and actin bundles, *Biophys. J.* 79 (2000) 1095–1106.
- [44] G.M. Lee, A. Ishihara, K.A. Jacobson, Direct observation of Brownian motion of lipids in a membrane, *Proc. Natl. Acad. Sci. U. S. A.* 88 (1991) 6274–6278.
- [45] T. Fujiwara, K. Ritchie, H. Murakoshi, K. Jacobson, A. Kusumi, Phospholipids undergo hop diffusion in compartmentalized cell membrane, *J. Cell Biol.* 157 (2002) 1071–1081.
- [46] E.D. Sheets, G.M. Lee, R. Simson, K. Jacobson, Transient confinement of a glycosylphosphatidylinositol-anchored protein in the plasma membrane, *Biochemist* 36 (1997) 12449–12458.
- [47] Q. Tang, M. Edidin, Lowering the barriers to random walks on the cell surface, *Biophys. J.* 84 (2003) 400–407.
- [48] K. Ritchie, A. Kusumi, Single-particle tracking image microscopy, *Method Enzymol.* 360 (2003) 618–634.
- [49] E.R. Weeks, J.C. Crocker, A.C. Levitt, A. Schofield, D.A. Weitz, Three-dimensional direct imaging of structural relaxation near the colloidal glass transition, *Science* 287 (2000) 627–631.
- [50] M.J. Saxton, Anomalous diffusion due to obstacles: a Monte Carlo study, *Biophys. J.* 66 (1994) 394–401.
- [51] M.J. Saxton, Anomalous diffusion due to binding: a Monte Carlo study, *Biophys. J.* 70 (1996) 1250–1262.
- [52] C. Dietrich, B. Yang, T. Fujiwara, A. Kusumi, K. Jacobson, Relationship of lipid rafts to transient confinement zones detected by single particle tracking, *Biophys. J.* 82 (2002) 274–284.
- [53] Y. Tseng, D. Wirtz, Mechanics and multiple-particle tracking microheterogeneity of alpha-actinin-cross-linked actin filament networks, *Biophys. J.* 81 (2001) 1643–1656.
- [54] T.G. Mason, K. Ganesan, J.H. van Zanten, D. Wirtz, S.C. Kuo, Particle tracking microrheology of complex fluids, *Phys. Rev. Lett.* 79 (1997) 3282–3285.
- [55] M. Oheim, W. Stuhmer, Tracking chromaffin granules on their way through the actin cortex, *Eur. Biophys. J.* 29 (2000) 67–89.
- [56] R.N. Ghosh, W.W. Webb, Automated detection and tracking of individual and clustered cell surface low density lipoprotein receptor molecules, *Biophys. J.* 66 (1994) 1301–1318.
- [57] J.C. Crocker, D.G.U. Grier, Methods of digital video microscopy for colloidal studies, *J. Colloid Interface Sci.* 179 (1996) 298–310.